Supplementary Information

Convenient Metal Embedment into Mesoporous Silica Channels for High Catalytic Performance on AB Dehydrogenation

Jin-Hyung Park,[a] Sung-Kwan Kim,[a] Han Sung Kim,[a] Yong Jae Cho,[a] Jeunghee Park,[a,] Kyung Eun Lee,[b] Chang Won Yoon,[c] Suk Woo Nam,[c] and Sang Ook Kang[a,*]*

Contents

Experimental details

Materials. Ammonia borane (AB) was purchased from Aviabor(Russian). Palladium acetate ($Pd(OAc)_2$), gold acetate ($Au(OAc)_3$), and silver acetate (Ag(OAc)) were purchased from Sigma-Aldrich. Tetraethylene glycol dimethyl ether (tetraglyme, TG; $C_{10}H_{22}O_5$) was purchased from Alfa Aesar. TG was purified by distillation method in order to remove water, air, and impurities. Pluronic P123($HO(CH_2CH_2O)_{20}(CH_2CH(CH_3)O)_{70}(CH_2CH_2O)_{20}H$; $EO_{20}PO_{70}EO_{20}$), Tetraethyl orthosilcate (TEOS; $Si(OC_2H_5)_4$), n-decane ($C_{10}H_{22}$), and ammonium fluoride (NH_4F) were purchased from Sigma-Aldrich. The deuterated solvent (C_6D_6) was dried through trap-to-trap distillation from Na metal and deoxygenated using three freeze-pump-thaw cycles.

Preparation of SBA-15. As a typical synthesis procedure [Reference: H. Zhang, J. Sun, D. Ma, X. Bao, A. Klein-Hoffmann, G. Weinberg, D. Su and R. Schlogl, *J. Am. Chem. Soc*., 2004, **126**, 7440], 2.4 g of P123 was dissolved in 84 mL of HCl solution (1.07 M) and then stirred at room temperature until the solution became clear. Different amounts of decane (with weight ratios of decane to P123 ranging from 0:1 to 7.6:1) were then added to the solution. The mixture was stirred at room temperature for at least 1 h. Finally, 0.027 g of NH_4F was added under stirring as a hydrolysis catalyst, followed by the addition of 5.1 g TEOS. The above mixture was stirred at 40 °C for 20 h and then transferred into an autoclave for further reaction at 100 °C for 48 h. The products were collected by filtration, dried in air and then in an oven at a temperature of 80 °C. The product was calcinated at 540 °C for 5 h to remove the templates. Samples of different weight ratios of decane to P123 were synthesized to obtain an optimized structure (decane:P123 = 5.8:1). The synthesized SBA-15 was characterized using XRD, N_2 adsorption-desorption isotherms, and TEM analyses.

Synthesis of Pd/SBA-15. $Pd(OAc)_2$ (0.1 g, 0.4 mmol) was dissolved in TG (20 mL), and SBA-15 (0.5 g) was then immersed in the $Pd(OAc)_2$/TG solution. The solution was stirred for 30 min under N_2 atmosphere at room temperature, and maintained at 220 °C for 30 min~4 h after the temperature elevation by heating in an oil bath. As the metal precursor was reduced to produce the metal nanoparticles, the color was changed from orange to black. The reaction solution was cooled to room temperature under N_2 atmosphere. The precipitates were separated by centrifugation (8000 rpm for 10 min) and washed with ethanol (10 mL) for the removal of the residual TG solvent, precursor, and TG-acetate. Finally, centrifugation was repeated three times, yielding a black powder consisting of PdNPs incorporated SBA-15.

Synthesis of Au/SBA-15 and Ag/SBA-15. After $Au(OAc)_3$ and SBA-15 were suspended in TG, the reaction mixture was heated to 150 °C for reduction of metal precursors. The reaction induced a distinct change in color from earth yellow to red. This significant color change presented direct evidence for the formation of AuNPs. Ag(OAc) and SBA-15 were suspended in TG, and the reaction mixture was heated to 150 ºC for reduction of metal precursors. The reaction induced a change in color; the production of Ag NPs turned the color from pale yellow to brown.

Kinetic profiles of dehydrogenation of AB. The apparatus used to measure hydrogen gas release has been previously eleborated [Reference: S. –K. Kim et al. *J. Am. Chem. Soc.*, 2010, **132**, 9954, Reference 19 of the manuscript: S. –K. Kim et al. *Chem. Commun.*, 2012, **48**, 2021.]. A mixture of AB (0.123 g) and TG (0.056 g) was placed in a two-necked round bottom flask, followed by the addition of supported catalyst (0.005 g) (Pd/SBA-15, Au/SBA-15, or Ag/SBA-15) through side arm attached to the reaction flask. This reaction flask was connected to a mineral-water-filled cylinder glass tube, and the amount of total hydrogen gas from liquid state AB with the catalytic reaction was recorded using a displaced volume of mineral-water in the tube. After AB dehydrogenation, the spent fuel was analysed by ^{11}B NMR.

Turnover Number (moles of produced H_2/moles of catalyst; TON) and Turnover Frequency (TON/unit time; TOF) values are calculated as follows:

1) Pd/SBA-15:

TON = 6.04 (1.51 equiv H_2 with 4 mmol of AB)/ 0.00370 mmol Pd[a)] = 1630

TOF = 1630/0.167 h (10 min) = 9760 h^{-1}

If thermal reaction (0.15 equiv H_2) contribution is subtracted, then TON = 1470 and TOF = 8800h^{-1}

[a)] 0.4 mmol Pd * 0.005 g catalyst / (0.5 g SBA-15 + 0.4 mmol Pd * 106.42 g/mol Pd * 1 mol / 1000 mmol)

2) PdNPs:

TON = 7.32 (1.83 equiv H_2 with 4 mmol of AB)/0.0470 mmol Pd = 156

TOF = 156/0.167 h (10 min) = 934 h^{-1}

If thermal reaction (0.15 equiv H_2) contribution is subtracted, then TON = 143 and TOF = 856 h^{-1}.

TOF of Pd/SBA-15 is higher by nearly 10 fold; 9760 h^{-1} versus 934 h^{-1} (if thermal decomposition of AB is ignored) and 8800 h^{-1} versus 856 h^{-1} (if thermal decomposition of AB is subtracted).

3) Au/SBA-15:

TON = 5.84 (1.46 equiv H_2 with 4 mmol AB)/0.00228 mmol Au[b)] = 2560

TOF = 2560/0.167 h (10 min) = 15300 h^{-1}

[b] 0.25 mmol Au * 0.005 g catalyst / (0.5 g SBA-15 + 0.25 mmol Au * 196.97 g/mol Au * 1 mol / 1000 mmol)
(0.05 g Au = 0.25 mmol Au) / 0.5 g SBA-15 * 100 = 10 wt% Au/SBA-15

4) Ag/SBA-15:
TON = 5.12 (1.28 equiv H_2 with 4 mmol of AB)/0.00418 mmol Ag[c] = 1220
TOF = 1220/0.167 h (=10 min) = 7300 h^{-1}
[c] 0.46 mmol Ag * 0.005 g catalyst / (0.5 g SBA-15 + 0.46 mmol Ag * 107.87 g/mol Ag * 1 mol / 1000 mmol)
(0.05 g Ag = 0.46 mmol Ag) / 0.5 g SBA-15 * 100 = 10 wt% Ag/SBA-15

Characterization.

(1) N_2 adsorption-desorption isotherms were measured at 77 K on a Micromeritics Tristar 3000 analyzer. Before the measurements, the sample was degassed at 300 ºC for 6 h. The specific surface area was calculated via the Brunauer-Emmett-Teller (BET) model at relative pressures of P/P_0 = 0.20. The total pore volume was estimated from the uptake of adsorbate at a relative pressure of P/P_0 = 0.99. Pore size distributions were derived from the adsorption branches of the isotherms using the Barrett-Joyner-Halenda (BJH) model.

(2) X-ray diffraction (XRD) was carried out in a Rigaku D/MAX-2500 V/PC using Cu Kα radiation (λ = 1.54056 Å) at 40 kV and 200 mA. The low-angle XRD patterns were collected at a scanning speed of 1°/min over a 2θ range of 0.5-6º, whereas the wide-angle XRD patterns were collected at a scanning speed of 4°/min over a 2θ range of 20-95º. Peak identification was made by comparison to the Joint Committee on the Powder Diffraction Standards card (JCPDS Card).

(3) Solution NMR spectra were collected at room temperature using a Mercury-300BB spectrometer (Varian Inc., Palo Alto, CA, USA) unless otherwise stated. The spectral frequency was 96.3 MHz for ^{11}B, and NMR shifts in ppm were reported with reference to external standards of $BF_3{\cdot}Et_2O$ for the ^{11}B nucleus.

(4) Transmission electron microscope (TEM) images were recorded on a Philips Tecnai G2 F20 system operated at 200 kV. Catalysts were sonicated in ethanol for 5 min, dropped on lacey carbon film coated copper grids (Ted Pella) and dried in air. For electron tomography (ET), the Pd/SBA-15 sample was embedded in Spurr's resin and cut using ultra-microtome (Reichert ultracut S, Leica). Its thick sections (200 nm) were collected onto a Quantifoil substrate copper grid. 5-nm gold particles (purchased from

Nanoprobes Co.) were affixed to the surface to serve as fiducial markers for the alignment. The grids were carbon coated to stabilize them under the electron beam, and placed in a Dual orientation Tomography Holder (model 927; Gatan Co.) and imaged in a Tecnai G2 operating at 200 kV. Images were acquired digitally using a 2048×2048 pixel charge-coupled device camera (Gatan) at a pixel size of 0.3 nm. Tilted TEM views were collected every 1º over a ±70º range. Tomographic reconstruction was carried out using the IMOD software package as described in the references [Reference: J. R. Kremer, D. N. Mastronarde and J. R. McIntosh, Computer visualization of three-dimensional image data using IMOD. *J. Struct. Biol.*, 1996, **116**, 71]. The tilted views were aligned using the positions of the gold particles, and tomograms were calculated using an R-weighted back projection algorithm. Tomographic reconstructions were shown and analyzed using the Amira 5.4 Program.

Density Function Theory (DFT) calculation for the $Pd(OAc)_2$:TG complex

All DFT calculations were performed with the Gaussian 09 package. The ground-state geometry of $Pd(OAc)_2$:TG has been optimized at the DFT level. Full geometry optimizations of the complexes in their singlet ground state were performed with DFT using the B3LYP functional,[1] with the relativistic effective core potential and basis set LanL2DZ for the palladium,[2] and the 6-31G basis set for the remaining atoms.[3] No symmetry constraints were applied during the geometry optimization.[4] The nature of located stationary points was further checked by computations of harmonic vibrational frequencies at the same level of theory. A static DFT calculation was performed to find the optimized structure of the $Pd(OAc)_2$:TG complex formed upon dissolution. Scheme S1 illustrates how initial TG interaction occurs with $Pd(OAc)_2$; TG is an open chain polyether and Pd/TG^i represents the most symmetrical structure imaginable for incoming $Pd(OAc)_2$. The optimized structure consists of an end-on, *O*-chelated structure with three oxygen atoms free from coordination, as represented by Pd/TG^o.

References

1. (a) C. Lee, W. Yang and R. G. Parr, *Phys. Rev. B*, 1988, **37**, 785. (b) S. H. Vosko, L. Wilk and M. Nusair, *Can. J. Phys.*, 1980, **58**, 1200. (c) A. D. Becke, *J. Chem. Phys.*, 1993, **98**, 5648. (d) P. J. Stephens, F. J. Devlin, C. F. Chabalowski and M. J. Frisch, *J. Phys. Chem.*, 1994, **98**, 11623.

2. P. J. Hay and W. R. Wadt, *J. Chem. Phys.*, 1985, ***82***, 299.

3. (a) "Gaussian Basis Sets for Molecular Calculations" S. Huzinaga, J. Andzelm, M. Klobukowski, E. Radzio-Andzelm, Y. Sakai and H. Tatewaki, Elsevier, Amsterdam, 1984. (b) E. R. Davidson and D. Feller, *Chem. Rev.*, 1986, **86**, 681.

4. M. J. Frisch, G. W. Trucks, H. B. Schlegel, G. E. Scuseria, M. A. Robb, J. R. Cheeseman, G. Scalmani, V. Barone, B. Mennucci, G. A. Petersson, H. Nakatsuji, M. Caricato, X. Li, H. P. Hratchian, A. F. Izmaylov, J. Bloino, G. Zheng, J. L. Sonnenberg, M. Hada, M. Ehara, K. Toyota, R. Fukuda, J. Hasegawa,

M. Ishida, T. Nakajima, Y. Honda, O. Kitao, H. Nakai, T. Vreven, Jr. J. A. Montgomery, J. E. Peralta, F. Ogliaro, M. Bearpark, J. J. Heyd, E. Brothers, K. N. Kudin, V. N. Staroverov, T. Keith, R. Kobayashi, J. Normand, K. Raghavachari, A. Rendell, J. C. Burant, S. S. Iyengar, J. Tomasi, M. Cossi, N. Rega, J. M. Millam, M. Klene, J. E. Knox, J. B. Cross, V. Bakken, C. Adamo, J. Jaramillo, R. Gomperts, R. E. Stratmann, O. Yazyev, A. J. Austin, R. Cammi, C. Pomelli, J. W. Ochterski, R. L. Martin, K. Morokuma, V. G. Zakrzewski, G. A. Voth, P. Salvador, J. J. Dannenberg, S. Dapprich, A. D. Daniels, O. Farkas, J. B. Foresman, J. V. Ortiz, J. Cioslowski and D. J. Fox, Gaussian 09, Revision B.01, Gaussian, Inc., Wallingford CT, 2010.

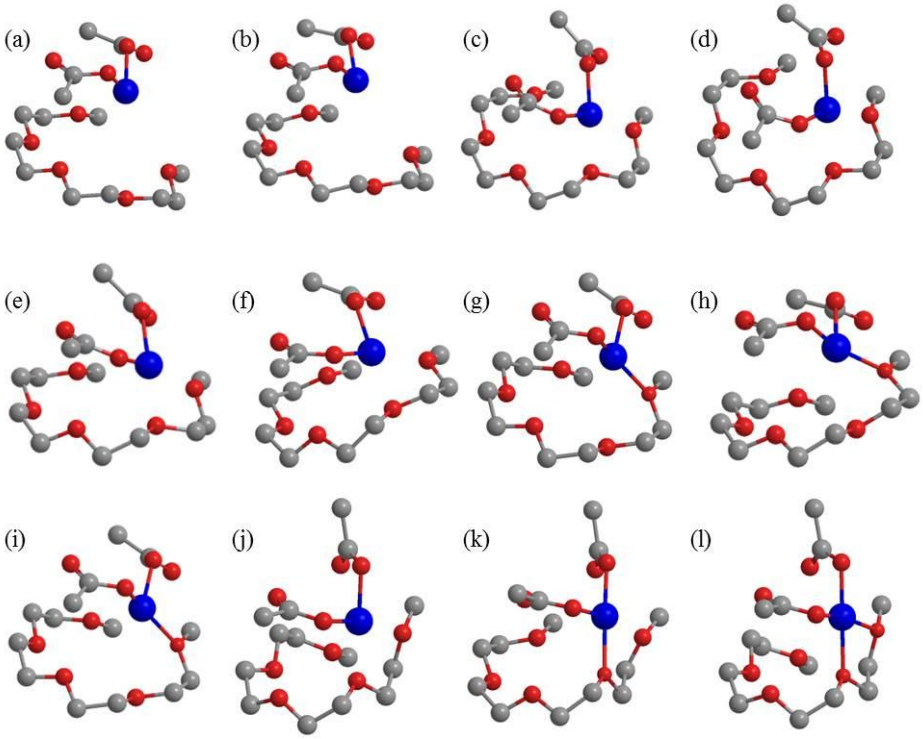

Chart S1: Molecular structure of $Pd(OAc)_2$:TG obtained by DFT calculation (in vacuum), started from the initial structure to the most stable structure.

Table S1. Optimized geometry parameters of $Pd(OAc)_2$:TG complex obtained by DFT calculation.[a]

No	Atom	X	Y	Z	No	Atom	X	Y	Z
1	O	-1.1026	0.4201	1.7363	27	H	3.6613	1.7919	3.3029
2	O	2.8193	0.3728	2.0242	28	H	3.9612	1.6732	0.8824
3	O	2.9276	-1.2304	-0.4100	29	H	4.6403	0.0351	1.0965
4	O	0.9001	-3.0764	-1.6094	30	H	3.7772	0.5099	-1.1759
5	O	-0.8097	-1.9265	0.3814	31	H	2.1276	0.6955	-0.5444
6	C	3.3941	0.7246	3.2680	32	H	3.9214	-1.7943	-2.1456
7	C	3.7098	0.6019	0.9335	33	H	2.2783	-1.1334	-2.3899
8	C	3.0852	0.1854	-0.3819	34	H	2.6036	-3.7066	-2.5965
9	C	2.8983	-1.7537	-1.7304	35	H	2.7316	-3.6929	-0.8220
10	C	2.3196	-3.1562	-1.6876	36	H	0.0281	-4.8781	-1.0112
11	C	0.2510	-3.8609	-0.6413	37	H	0.8669	-3.9691	0.2654
12	C	-1.0606	-3.1695	-0.3080	38	H	-1.6826	-3.7794	0.3583
13	C	-0.8437	-1.9528	1.8124	39	H	-1.5918	-2.9166	-1.2273
14	C	-0.2968	-0.6300	2.3080	40	H	-0.1721	-2.7602	2.1288
15	C	-0.7752	1.7309	2.2406	41	H	-1.8955	-2.0847	2.1008
16	Pd	-1.2140	0.0300	-0.4156	42	H	-0.3872	-0.5895	3.4021
17	O	-1.5260	-0.7086	-2.2425	43	H	0.7522	-0.4969	2.0200
18	C	-0.6006	-0.4976	-3.1556	44	H	-1.4726	2.4186	1.7654
19	C	-0.8993	-1.2526	-4.4464	45	H	-0.9232	1.7335	3.3271
20	O	0.4113	0.1786	-3.0160	46	H	0.2470	1.9974	1.9690
21	O	-1.5576	1.8752	-1.0998	47	H	-1.9691	-1.2662	-4.6659
22	C	-0.5219	2.6820	-1.0539	48	H	-0.5625	-2.2877	-4.3227
23	C	-0.7311	3.9355	-1.8910	49	H	-0.3461	-0.7988	-5.2702
24	O	0.5166	2.4831	-0.4257	50	H	-0.0548	4.7230	-1.5543
25	H	2.6515	0.5213	4.0442	51	H	-0.4990	3.6910	-2.9330
26	H	4.2982	0.1327	3.4773	52	H	-1.7688	4.2745	-1.8500

[a]Cartesian coordinates

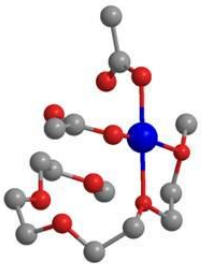

Optimized geometry of $Pd(OAc)_2$:TG

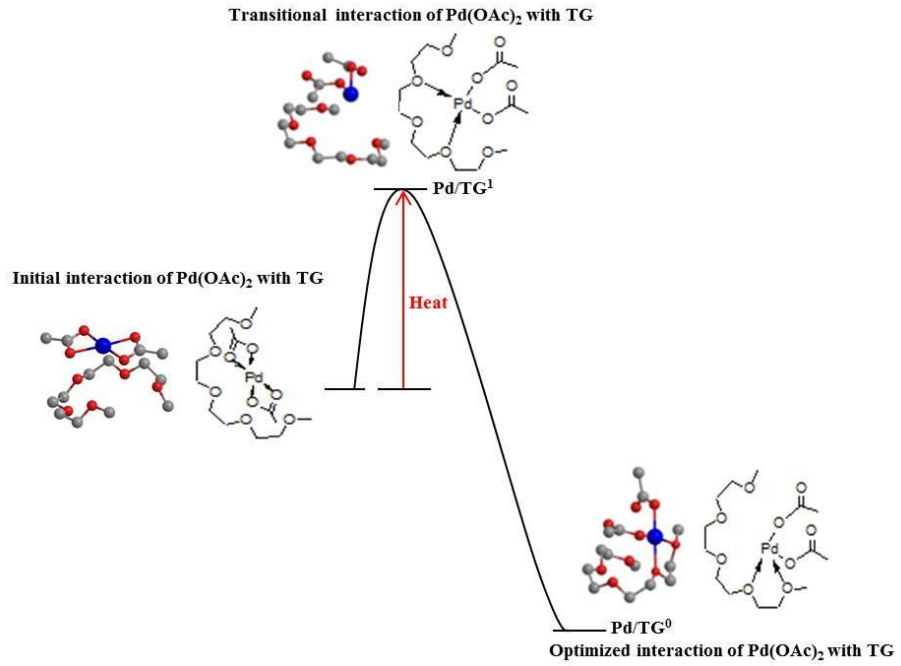

Scheme S1: Initial interaction of $Pd(OAc)_2$ with TG (Pd/TG^i) and the respective thermally-induced, optimized geometry showing end-on ether interaction, Pd/TG^o.

Once the potential Pd precursor was tethered by TG, Pd/TG^o, came into contact with the interior of SBA-15, which bears terminal Si-OH groups. Secondary signature interaction might be foreseeable with the tethered polyetheral units of the Pd precursor, Pd/TG^o. Impregnation into silica channels can be further expected via capillary effects that are well explained by previous examples. This procedure is portrayed as the Scheme S2 diagram.

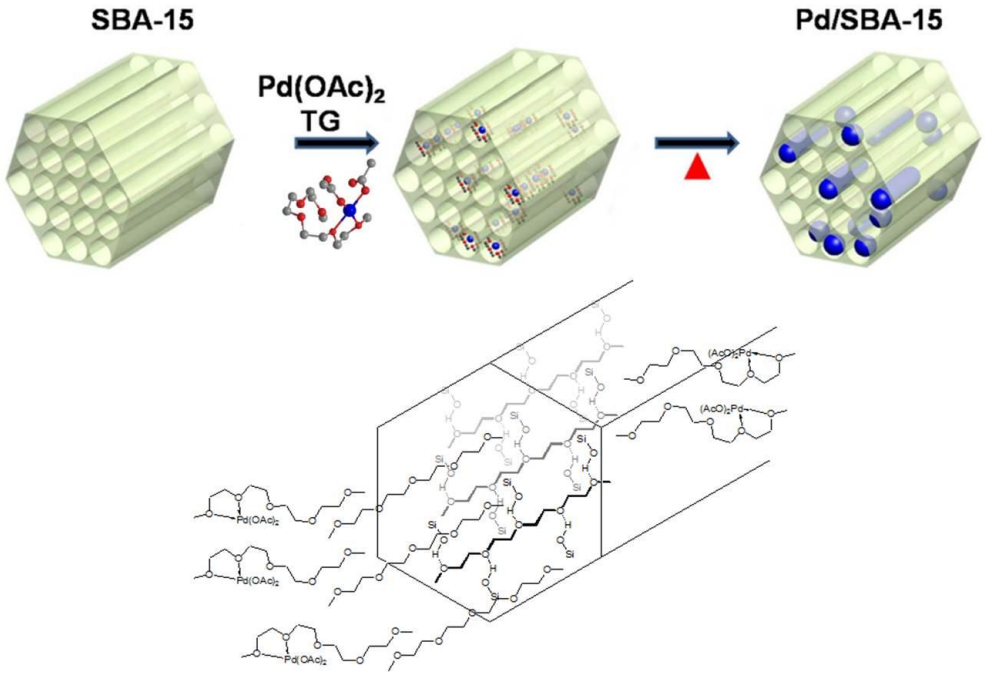

Scheme S2. Pd/TG^o passing through the SBA-15 channels via capillary effect.

Table S2. Pore structure parameters of SBA-15 and Pd/SBA-15 samples derived from the N_2 adsorption-desorption isotherms

Sample	S_{BET}(m^2/g)[b]	V_{BJH}(cm^3/g)[c]	D_{BJH}(nm)[d]	d_{100}(nm)[e]	a_0(nm)[f]	t(nm)[g]
SBA-15	724.95	1.34	7.43	12.8	14.8	7.37
Pd/SBA-15	619.62	1.21	7.22	12.8	14.8	7.58

[a]The metal amount is 10.0 wt%; [b]BET specific surface area; [c]BJH pore volume; [d]BJH average pore diameter; [e]Periodicity of host SBA-15 derived from low-angle XRD (see Figure S1); [f]The unit cell parameter, $a_0 = 2d_{100}/\sqrt{3}$; [g]The pore wall thickness, $t = a_0 - D_{BJH}$.

The reduction of Brunauer-Emmett-Teller (BET) surface areas, Barrett–Joy–Halenda (BJH) pore volume, and average pore size, together with the increased thickness of the pore walls in the Pd/SBA-15 sample can be attributed to the incorporation of PdNPs in the channels of SBA-15. This suggests that the incorporated PdNPs occupy the channels of the host silica and the majority of them remain open.

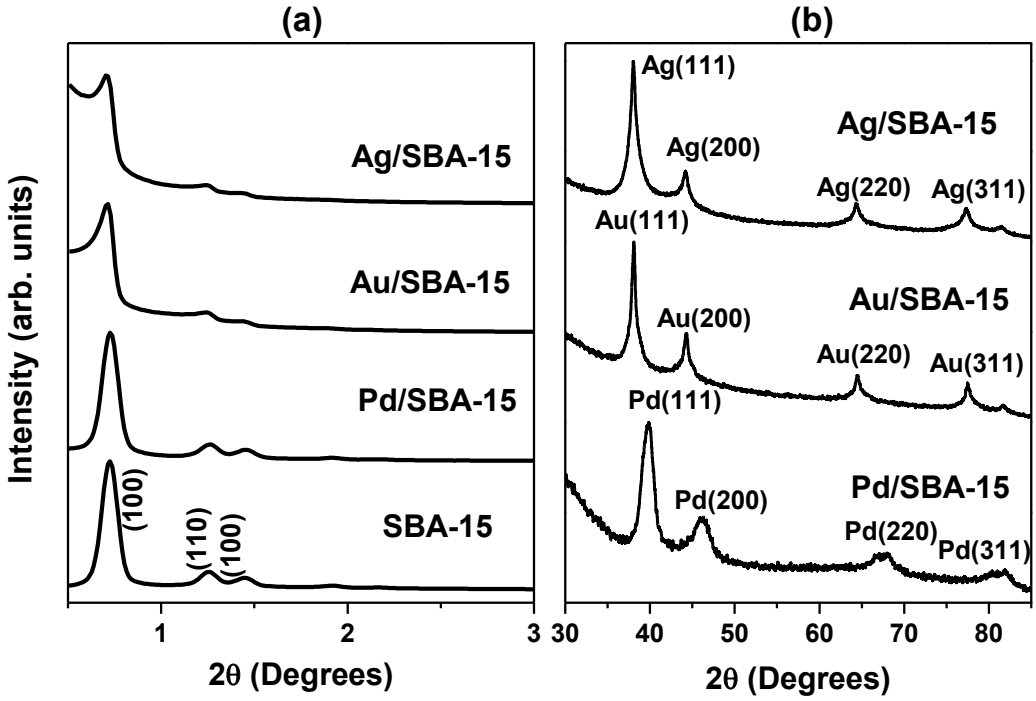

Figure S1. (a) Low-angle and (b) wide-angle XRD patterns of SBA-15, Pd/SBA-15, Au/SBA-15, and Ag/SBA-15.

All peaks at low angle are pertinent to the matrix, SBA-15. From the position of (100) peak (2θ =0.715°), we estimated the *d*-spacing of (100) planes to be 12.8 nm. A wide-angle XRD pattern of Pd/SBA-15 shows four peaks at 2θ = 40.02°, 46.29°, 67.99°, and 81.90°, assignable to (111), (200), (220), and (311) of cubic Pd (JCPDS Card File No.46-1043), respectively. Four peaks of Au/SBA-15 at 2θ = 38.09°, 44.25°, 64.45°, and 77.48° are assigned (111), (200), (220), and (311) of cubic Au (JCPDS Card No. 04-0784), respectively. The peaks of Ag/SBA-15 at 2θ = 38.04°, 44.2°, 64.35°, and 77.29° can be indexed to the (111), (200), (220), and (311) planes of cubic Ag (JCPDS Card File No. 04-0783), respectively.

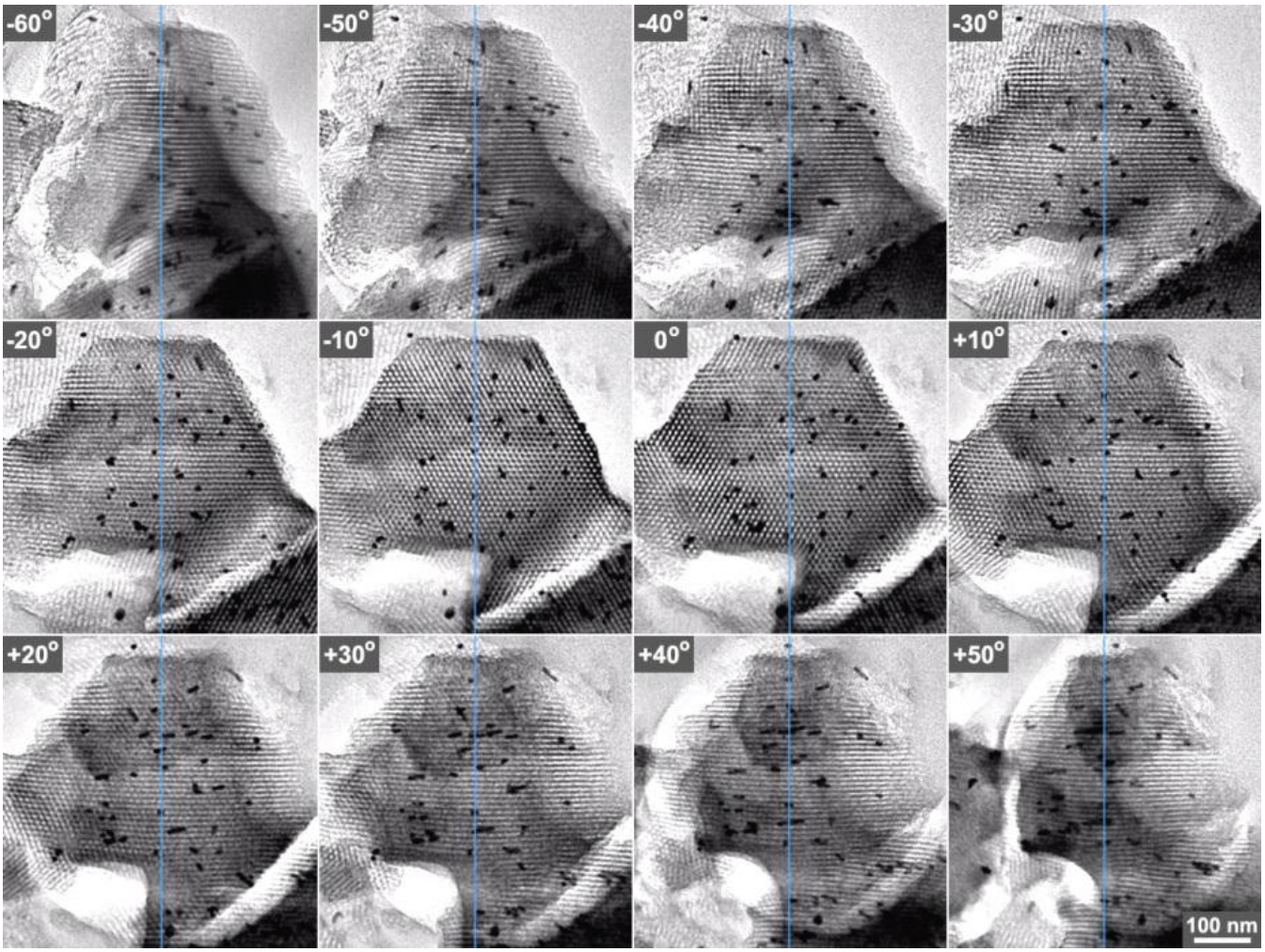

Figure S2. Snapshots of Movie 1; A series of TEM images, as Pd/SBA-15 nanostructure rotates from -60° to 50°.

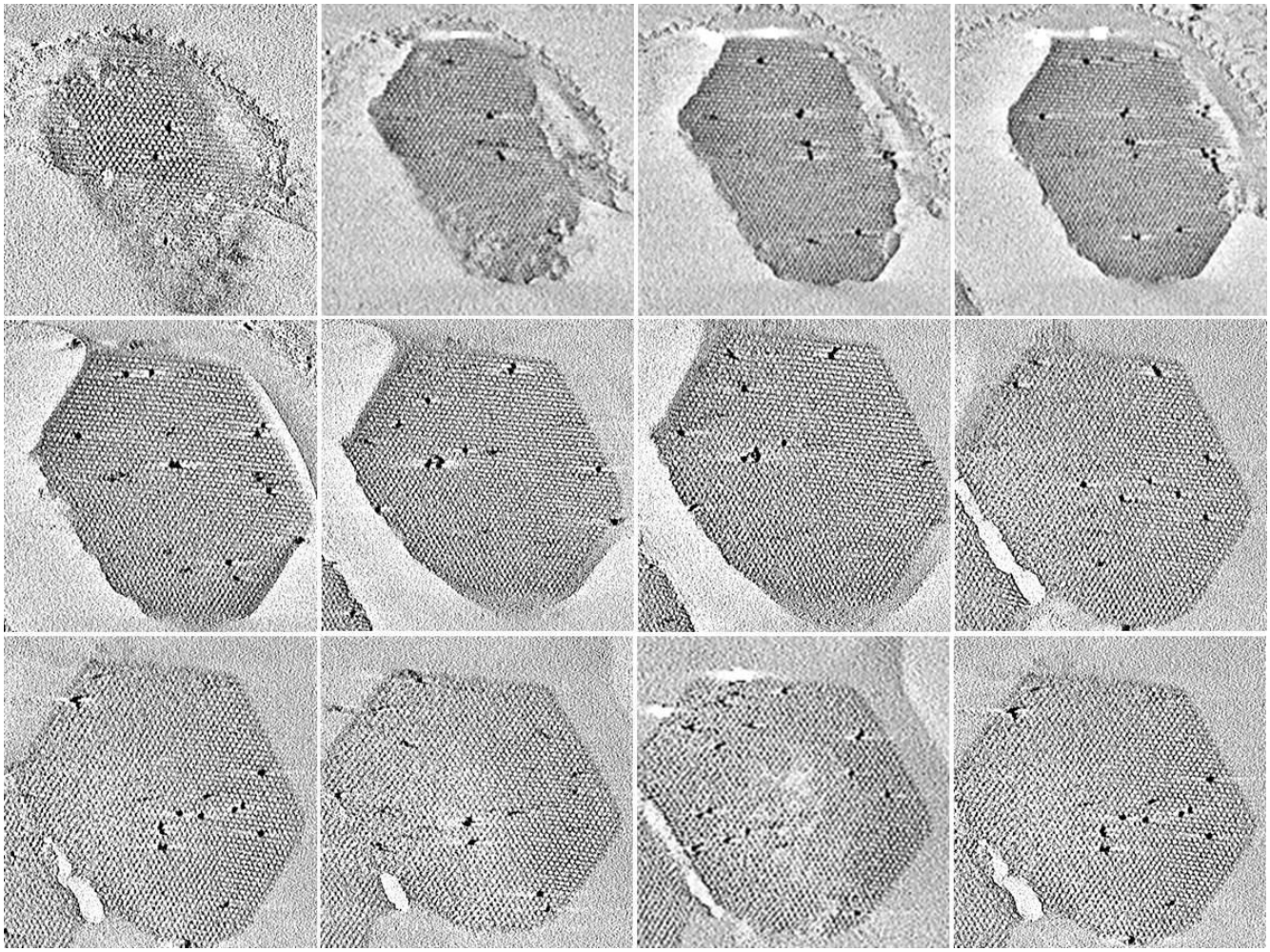

Figure S3. Snapshots of Movie 2; Projections of an orthogonal XY cross-section (2D orthoslice method) of the 3D reconstruction taken along the [001] zone axis of the SBA-15 matrix.

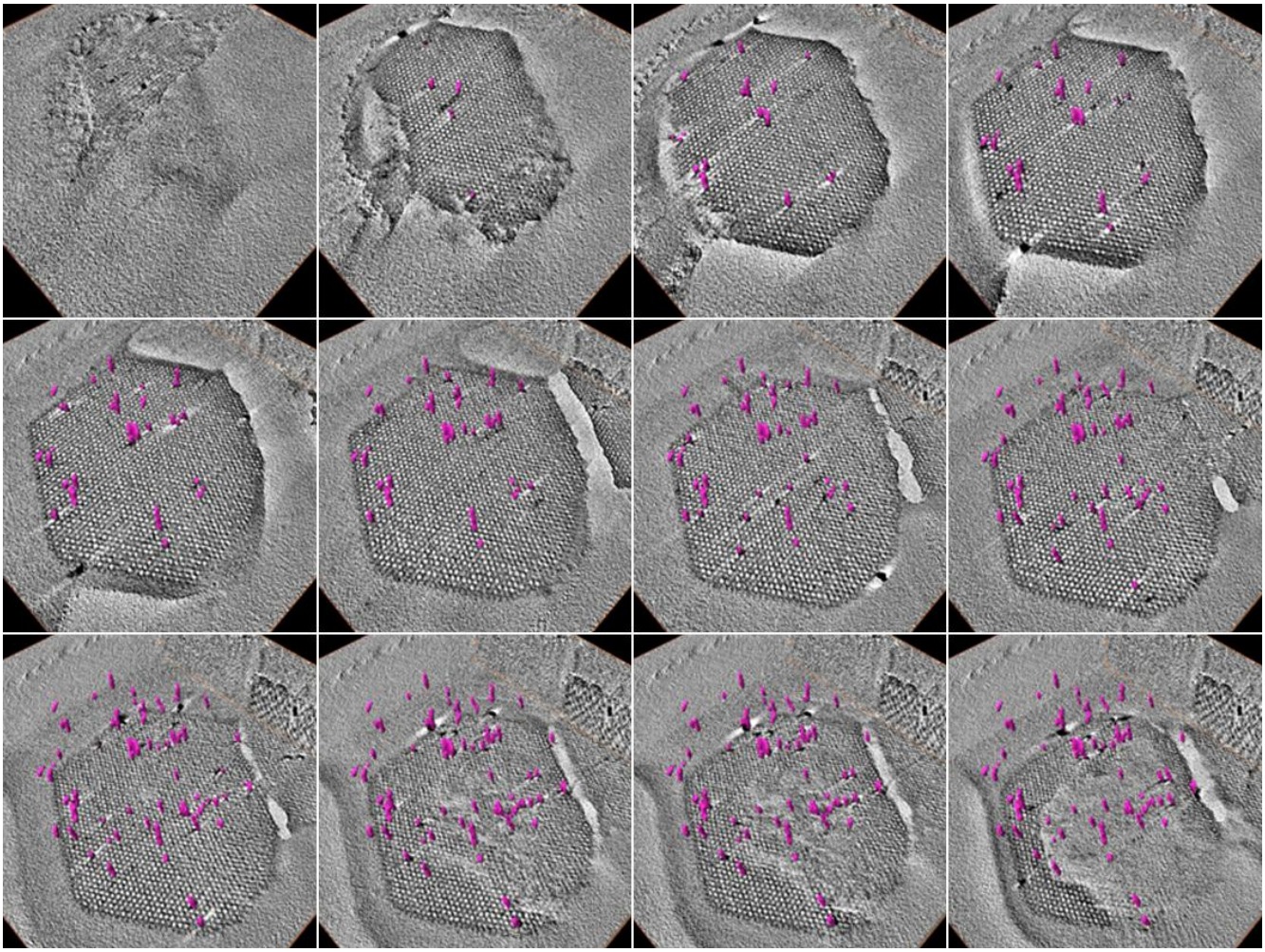

Figure S4. Snapshots of Movie 3; orthogonal XYZ cross-section (3D orthoslice method) data through the 3D reconstruction, showing the extraction of PdNPs (pink colored) from the SBA-15 frame.

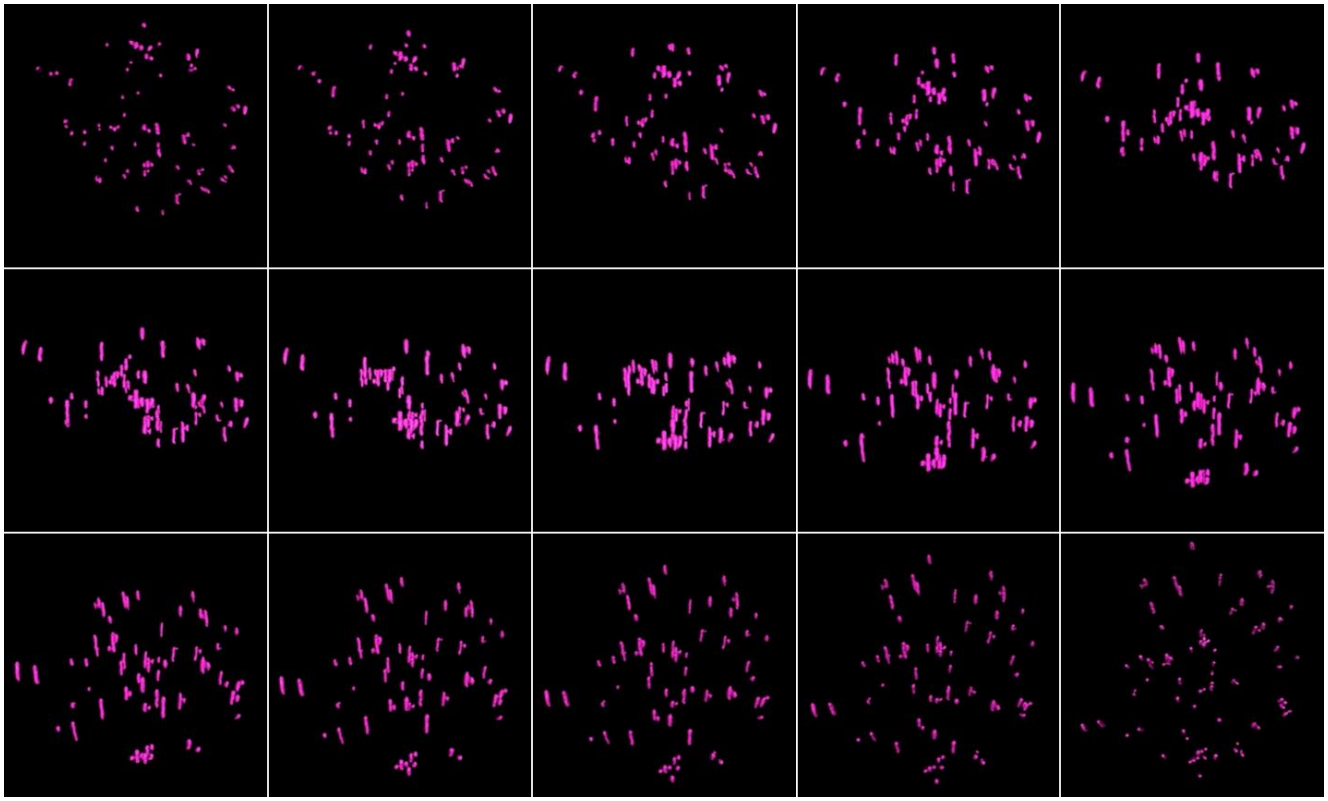

Figure S5. Snapshots of Movie 4; a series of rotation views of the extracted PdNPs.

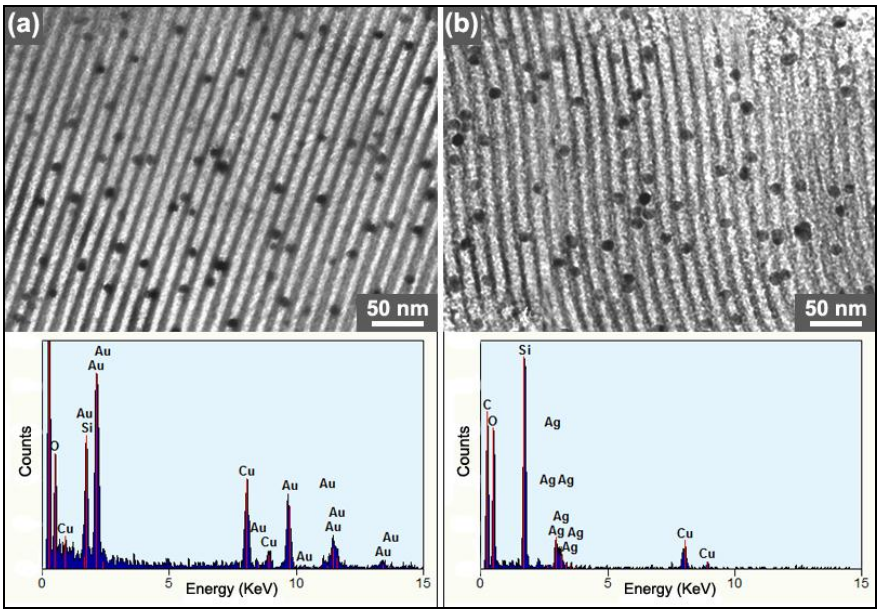

Figure S6. TEM images and EDX data of (a) Au/SBA-15 and (b) Ag/SBA-15. AuNPs and AgNPs with 10 wt% were encapsulated in the SBA-15.

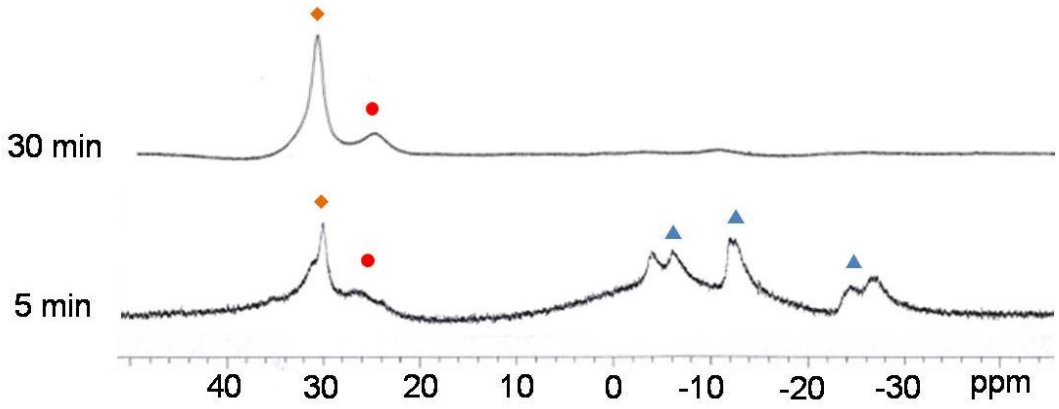

Figure S7. ^{11}B NMR spectra of spent fuel obtained after AB dehydrogenation (96.3 MHz); ◆borazine; ●PB (polyborazylene); ▲B-(cyclodiborazanyl)aminoborohydride (BCDB). Evolution of the spectrum was recorded after 5 min and 30 min reaction times using Pd/SBA-15 with AB dissolving TG at 90 °C. The spectrum showed a strong resonance at 30 ppm and a weak resonance at 25 ppm, which were assignable to borazine and polyborazylene, respectively.

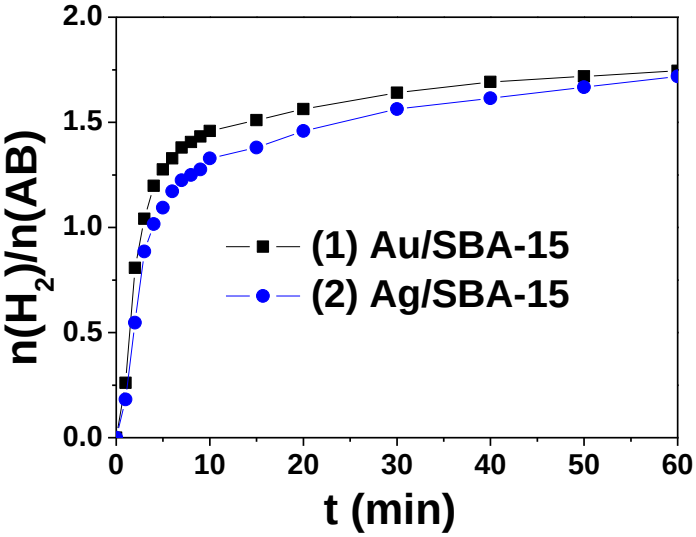

Figure S8. Hydrogen generation of AB/TG mixture using 10 wt% metal encapsulated Au/SBA-15 and Ag/SBA-15 at 90 °C. Au/SBA-15 and Ag/SBA-15 exhibited excellent kinetics for AB dehydrogenation, completing a 1.7 equiv H_2 release for 1 h. The catalyst system consists of 0.123 g (4 mmol) AB, 0.056 g TG, and 0.005 g Au/SBA-15 (or Ag/SBA-15). Initial TOF (for 10 min) is as high as 15300 and 7300 h^{-1} for Au/SBA-15 and Ag/SBA-15, respectively.

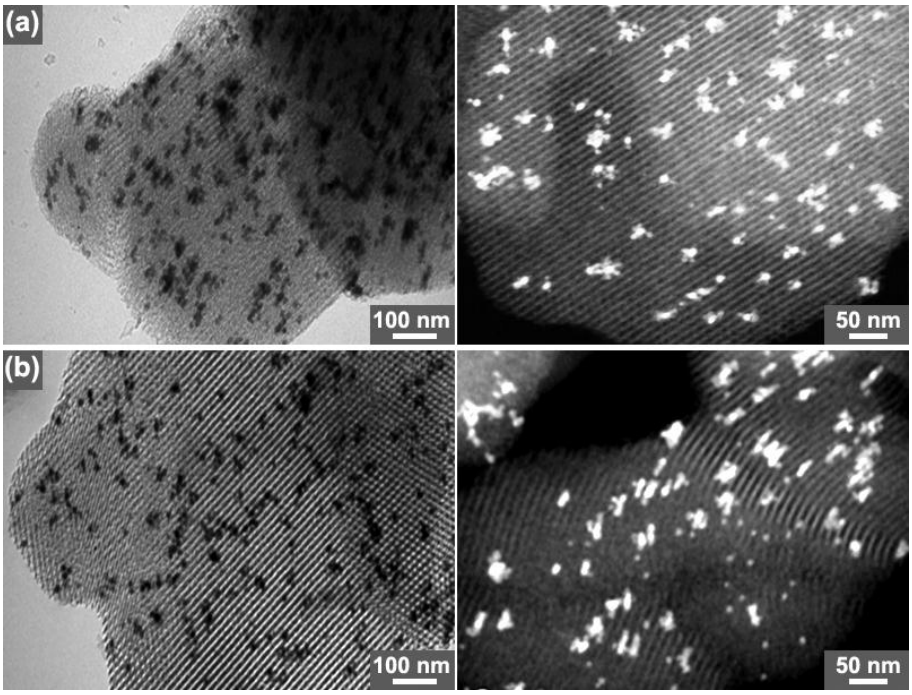

Figure S9. TEM and scanning TEM (STEM) images of Pd/SBA-15 (a) before and (b) after AB dehydrogenation (5 runs). After dehydrogenation and removal of the BN residues coated on the catalyst surface by immersion in methanol, PdNPs impregnation in SBA-15 channels had not changed significantly. The size, morphology, and structure of PdNPs were kept constant.

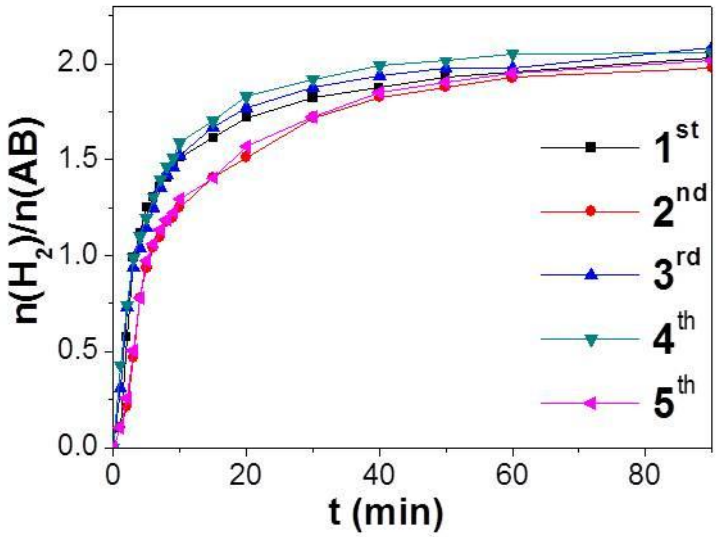

Figure S10. Recycle test for the used Pd/SBA-15 catalysts in situ generated from the spent fuels.

Recycle tests were performed for the catalyst samples regenerated in situ from the spent fuels. Thus, spent fuels were washed at least ten times with methanol (15 ml) using centrifuge (8000 rpm, 10 min) to give the catalyst for the subsequent recycle run. When AB dehydrogenation activity of the fifth run was compared with that of the first run, no discernible activity decrease was noted.